TRENDS IN SCIENCES 2025; 22(8): 10210
https://doi.org/10.48048/tis.2025.10210 RESEARCH ARTICLE

Pathavi Apo Vayo Formulary Extract Treatment Under High Glucose Conditions on Foam Cell Formation in RAW264.7 Macrophages

Bung-on Prajanban[1,*] Orapun Jaisamut[2], Sittiruk Roytrakul[3] and Niramai Fangkrathok[4]

[1]Faculty of Agricultural Technology, Burapha University Sakaeo Campus, Sa Kaeo 27160, Thailand
[2]Faculty of Science and Technology, Rajamangala University of Technology Tawa-Ok, Chonburi 20110, Thailand
[3]Functional Proteomics Technology Laboratory, National Center for Genetic Engineering and Biotechnology, National Science and Technology Development Agency, 113 Thailand Science Park, Pathumthani 12120, Thailand
[4]Center for Research and Development of Herbal Health Products, Faculty of Pharmaceutical Sciences, Khon Kaen University, Khon Kaen 40002, Thailand

([*]Corresponding author's e-mail: bungon.pr@buu.ac.th)

Received: 19 March 2025, Revised: 24 April 2025, Accepted: 1 May 2025, Published: 25 June 2025

Abstract

The objective of the present study was to investigate the effect of Pathavi Apo Vayo formulary extract (PAV) extracted by 50% ethanol on foam cell formation of macrophages (RAW264.7), in high glucose medium (HGM). Foam cell formation and lipid accumulation, gene expression, cytokine production, proteomic analysis, protein difference and protein-chemical correlation were studied using Oil Red O staining, Real-Time PCR, ELISA, Liquid Chromatography-Tandem Mass Spectrometry (LC/MS-MS), and bioinformatics (Venn diagram and STITCH), respectively. Oxidized low-density lipoprotein (oxLDL) was used to induce the formation of foam cells. In oxLDL induction, PAV co-treatment suppressed lipid accumulation in foam cells slightly, while a higher concentration of PAV (200 - 400 µg/mL) increased the lipid accumulation in the treated cells slightly. Similarly, PAV up-regulated the gene expressions of oxLDL receptors including LOX-1. However, PAV down-regulated the expression of pro-inflammatory cytokine genes including TNF-α. In addition, PAV also decreased cytokine production after co-treatment with oxLDL and LPS in both normal glucose medium (NGM) and HGM. In total 7,192 proteins were identified from 6 glucose medium conditions using shotgun proteome analysis, 42 of which were expressed only in HGM and HGM +400 µg/mL PAV conditions. A proteome mechanism during the process of PAV treatment under high glucose conditions is proposed. In conclusion, PAV could slightly decrease foam cell formation, but might increase lipid accumulation in foam cells when using higher concentrations. Therefore, this traditional medicine should be used carefully in hyperlipidemia and diabetes patients.

Keywords: Pathavi Apo Vayo formulary, High glucose, oxLDL, Foam cell, LOX-1, Proteomics

Introduction

Diabetes and atherosclerosis are increasingly becoming global public health concerns. Atherosclerosis is the major cause of cardiovascular events, and an elevated level of circulating modified low-density lipoprotein (LDL) is a known risk factor of cardiovascular diseases [1]. Diabetes mellitus comprises a group of carbohydrate metabolism disorders that share a common main feature of chronic hyperglycemia from the defects of insulin secretion, insulin action, or both. Atherosclerosis is one of the most dangerous vascular complications of diabetes, a leading cause of morbidity and disability in type 1 and/or type 2 diabetes patients. Atherosclerosis risk in diabetic patients is obviously higher than that of non-diabetic individuals [2]. In addition, diabetes mellitus and atherosclerosis presentations are connected through several pathological pathways. Among the factors, the acceleration, dyslipidemia with increased levels of atherogenic LDL, hyperglycemia, oxidative stress, and increased inflammation are proposed [1]. Diabetes

mellitus possibly affects the atherogenic process and its relationship with chronic inflammation [1]. One mechanism by which high glucose conditions may enhance this process involves the activation of Nuclear Factor-κB (NF-κB), which leads to the expression of several inflammatory genes including adhesion molecules that facilitate monocyte adhesion to endothelial cells. Monocytes then differentiate into macrophages, which take up lipids (thereby becoming foam cells) and accumulate in the artery wall in diabetes, resulting in accelerated fatty streak formation [3].

Macrophages are the key players in all stages of atherogenesis. Formation of foam cells that occurs in the initial stages of atherogenesis is a hallmark of atherosclerotic disease. Macrophages internalize oxidized low-density lipoprotein (oxLDL) by several scavenger receptors (SRs), such as SR-A1 and lectin-like oxLDL receptor-1 (LOX-1), resulting in lipid accumulation and transformation into foam cells. LOX-1 expression in macrophages can be upregulated by several stimuli, including oxLDL, high-glucose levels, and proinflammatory cytokines [4]. LOX-1 gene inactivation does not markedly modify oxLDL uptake in unstimulated macrophages, as LOX-1 accounts for 5% - 10% of oxLDL uptake by these cells. However, when LOX-1 is upregulated, internalization of oxLDL increases by more than 40% [5]. High glucose concentrations enhance LOX-1 expression in human monocyte-derived macrophage; this effect is associated with foam cell formation through a LOX-1 - dependent pathway [6]. LOX-1 expression can also be induced by lipopolysaccharide (LPS) [7] and TNF-α [8]. In macrophages, SR-A1 is involved in the uptake of modified LDL. Moreover, pro-inflammatory cytokines, such as tumor necrosis factor α (TNF-α), promote SR-A1 expression by the activation of NF-κB transcription [9]. TNF-α enhances foam cell formation in macrophages, in part by inhibition of intracellular lipid catabolism [10]. Inhibition of this cytokine decreases oxLDL accumulation and foam cell formation [11].

Many synthetic drugs for diabetes have been developed, and yet a complete cure is not provided by any of the molecules. Once-daily metformin extended-release does not only improve measures of glycemic control in Asian patients with type 2 diabetes mellitus (T2DM) but also has a favorable gastrointestinal tolerability profile [12]. Continuous use of some synthetic agents causes severe side effects, and thus the demand for non-toxic, affordable drugs persists. An appropriate strategy for the prevention and treatment of diabetic atherosclerosis is necessary. Therefore, it is important to identify pharmaceutical agents to inhibit diabetes-accelerated atherosclerotic diseases. Traditional medicinal plants and natural products are considered as alternative therapeutic strategies for the treatment of diabetic atherosclerosis with lower costs and fewer side effects [2]. Natural compounds such as curcumin, berberine, resveratrol, salidroside and ginkgo biloba are used as potential agents for diabetic atherosclerosis treatment [2]. Moreover, traditional Chinese herbal medicine such as *Salvia miltiorrhiza*, Salvianolic acid and Celastrol have been used to treat diabetes and atherosclerosis [2].

Medicinal plants are used in Thailand for treating diabetes, as well as their hypoglycaemic pharmacological evidence and potential therapeutic nature being used for diabetes-related complications [13]. Thai traditional herbal formulae, Sattagavata, Mathurameha and Tubpikarn have been prescribed for diabetic patients for a long time. The combined Thai anti-diabetic herbal formula has an anti-hyperglycemic action in the Type II diabetic animal model [14]. Pathavi Apo Vayo formulary (PAV) is one Thai traditional medicine from Wat Phra Chetuphon's inscriptions. This formulary consists of 21 herbs and has been used for the treatment of diabetes. In the diabetes model, the blood sugar level of diabetic rats was significantly decreased after treating with PAV for 12 weeks. In addition, the levels of cholesterol, LDL and TNF-α in blood were also significantly decreased after treatment (unpublished data). Therefore, the chemical composition of PAV and its effect on pro-inflammatory mediators and foam cell formation using a model of diabetes-induced atherosclerosis has been continuously studied. The chemical composition of plant extracts such as remaining content in PAV extract and gallic acid can be used as chemical markers. This PAV extract had low cytotoxicity and inhibited NO production in the normal glucose medium (NGM) and high glucose medium (HGM), but without a statistical difference [15]. Understanding the role of PAV on macrophages that are related to inflammation, hyperglycemic condition and foam cell formation in diabetes offers

hope for new treatment strategies to reduce diabetes' leading causes of atherosclerosis. The proteomic approach has been widely used to investigate protein alteration in various organisms, because it provides the entire data network of protein regulation. In addition, this technique can be used to detect the proteins regulated by post-translational modification [16]. Using large-scale proteomics, identified potential candidate biomarkers of plant-based diets and pathways may partially explain the associations between plant-based diets and chronic conditions [17]. In a previous report, the 47 identified plasma proteins predictive of incident diabetes established causal effects for 3 proteins, and identified diabetes-associated inflammation and lipid pathways with potential implications for diagnosis and therapy [18].

Therefore, the aim of this study was to investigate the effect of PAV that was extracted by 50% ethanol on foam cell formation in HGM conditions in macrophages (RAW264.7). A standard medicine for hyperlipidemia treatment, Simvastatin (Svt), which has been reported to inhibit foam cell formation and inflammatory responses [19-22] was selected to compare the bioactivity with PAV in this study. Foam cell formation and lipid accumulation, gene expression, cytokine production, proteomic analysis, protein difference and protein-chemical correlation were studied using Oil Red O staining, Real-Time PCR, ELISA, Liquid Chromatography-Tandem Mass Spectrometry (LC/MS-MS), and bioinformatics (Venn diagram and STITCH), respectively.

Materials and methods

Preparation of Pathavi Apo Vayo formulary extracts

PAV was purchased from Bansamunpaiosot, Bangkok, Thailand [15]. It was macerated in 50% ethanol for 7 days, then filtered. The residue after maceration was repeatedly macerated in 50% ethanol for 7 days. The filtrates were then combined and the solvent was evaporated and concentrated using a rotary evaporator.

Determination of foam cell formation

RAW264.7 cells were cultured in NGM (Dulbecco's Modified Eagle Medium (DMEM) supplemented with 10% fetal bovine serum, 2 mM L-glutamine and 5.5 mM D-glucose) or HGM (DMEM supplemented with 10% fetal bovine serum, 2 mM L-glutamine and 15 mM D-glucose) and then incubated at 37 °C and 5% CO_2 for 7 day. PAV (0 - 400 µg/mL) or 10 - 40 µM simvastatin (Svt) were diluted with NGM or HGM and then added into the cells (2×10^5 cells/well) in the absence or presence of 50 µg/mL oxLDL and 10 µg/mL lipopolysaccharides (LPS). The cells were then incubated at 37 °C and 5% CO_2 for 24 h. The treated cells were analyzed for lipid accumulation in foam cells using Oil Red O staining. The stained cells were photographed and intensity determined at 540 nm.

Real-time PCR

The treated RAW264.7 cells were harvested and extracted for total RNA using E.Z.N.A.® Total RNA Kit (Omega Bio-tek, GA) according to the manufacturer's instruction. For the synthesis of cDNA, total RNA was treated with DNase I. FIREScript RT cDNA synthesis kit and Oligo-dT primers (Solis BioDyne, Estonia) were used according to the manufacturer's instruction. Samples were prepared using Hot FIREPol® EvaGreen ® qPCR Mix Plus (no ROX) (Solis BioDyne, Estonia) according to the manufacturer's instruction and run on a CFX96 Touch Real-Time PCR Detection System (Bio-Rad). The cDNA (2.5 ng) was amplified using the specific primers for β-actin, LOX-1, SR-A1 and TNF-α (**Table 1**). The genes were amplified by Real-Time PCR in triplicate. The process for the Real-Time PCR reaction was as follows; initial activation at 95°C for 12 min, followed by 40 cycles of denaturation at 95°C for 15 s, annealing at 54°C for 20 s and elongation at 72°C for 20 s. Fold changes of gene expression were calculated using the $2^{-\Delta\Delta CT}$ method. The methods for the calculation were as follows [23].

ΔCT = CT (target) – CT (reference)
$\Delta\Delta CT$ = CT (test sample) – CT (control sample)

Moreover, each cDNA sample (1 µL) as a template was mixed with Tag DNA polymerase recombinant (Invitrogen, Brazil), each primer and the deoxynucleotide mix. Amplification was completed using 30 cycles and the PCR amplification followed as described in Tag DNA polymerase recombinant

protocol (Invitrogen, Brazil). PCR products were then visualized with 1.5% agarose gel, using FluoroVueTM nucleic acid gel staining (SMOBIO Technology, Inc., Taiwan).

Table 1 Oligonucleotide primers used in real time PCR.

Gene		Primer Sequence (5′-3′)	References
LOX-1	Forward	CAGCGAACACAGCTCCGTCTTGAAGG	[5]
	Reverse	GGCCAACCATGGCTTGGGAGAATGG	
SR-A1	Forward	TGGTCCACCTGGTGCTCC	[24]
	Reverse	ACCTCCAGGGAAGCCAATTT	
TNF-α	Forward	ATGAGCACAGAAAGCATGATC	[25]
	Reverse	TACAGGCTTGTCACTCGAATT	
β-actin	Forward	TCATGAAGTGTGACGTTGACATCCGT	[25]
	Reverse	CCTAGAAGCATTTGCGGTGCACGATG	

Determination of TNF-α production

Determination of foam cell formation by the treated culture medium was taken for measurement of TNF-α production using an enzyme-linked immunosorbent assay (ELISA) kit following the protocol as described in DuoSet® ELISA kit standard protocol.

Protein preparation and digestion

RAW264.7 (1×10^5 cells/well) were seeded and incubated at 37 °C and 5% CO_2 for 24 h. Extracts were diluted with HGM in the absence or presence of oxLDL and LPS. After incubation at 37 °C and 5% CO_2 for 24 h, the culture media was removed. Cells were ground to powder in liquid nitrogen and extracted with 0.5% SDS. Protein concentration was determined by the Lowry method. Protein samples (5 µg) were subjected to in-solution digestion. For digestion, samples were mixed with 50 ng/µL of sequencing grade trypsin (Promega, Germany) in the ratio of 1:20, and then incubated at 37 °C overnight. The digested samples were dried and protonated with 0.1% formic acid. The samples were then injected into LC-MS/MS.

Bioinformatics and data analysis

MaxQuant 1.6.6.0 was used to quantify the proteins in individual samples using the Andromeda search engine to correlate MS/MS spectra to the Uniprot Mus musculus database. Label-free quantitation with MaxQuant's standard settings was performed. Peptides with a minimum of 7 amino acids and at least one unique peptide were required for protein identification. Proteins, with at least 2 peptides and at least one unique peptide, were considered as being identified and used for further data analysis. Protein FDR was set at 1% and estimated by using the reversed search sequences. The maximal number of modifications per peptide was set to 5. As a FASTA file search, the proteins presented in the *Mus musculus* proteome were downloaded from Uniprot. Potential contaminants presented in the contaminants FASTA file that comes with MaxQuant were automatically added to the search space by the software.

The MaxQuant ProteinGroups.txt file was loaded into Perseus version 1.6.6.0 [26]; potential contaminants that did not correspond to any UPS1 protein were removed from the data set. Max intensities were $\log_2$ transformed and pairwise comparisons between conditions were done via t-tests. Missing values were also imputed in Perseus using constant value (0). The visualization and statistical analyses were conducted using the MultiExperiment Viewer (MeV) in the TM4 suite software [27]. Protein organization and biological action were investigated conforming to protein analysis through evolutionary relationships (Panther) protein classification [28]. A Venn diagram was used to show the differences between protein lists originating from differential analyses [29]. The STITCH database version 5 was used to analyze the common and the predicted functional interaction networks between identified proteins and small molecules [30].

Statistical analysis

All data results are representative of 3 independent experiments and values are expressed as mean ± SD. Statistical analysis was performed using SPSS. Data were analyzed by one-way ANOVA and multiple comparison (LSD) for investigating significant differences ($p < 0.05$).

Results and discussion

Foam cell formation

PAV is one of the Thai traditional medicines and consists of 21 herbal plant powders. It has been used in the treatment of diabetic patients. PAV extract shows low cytotoxicity and could inhibit NO production in NGM and HGM without a statistical difference [15]. Nitric oxide synthase 1 (NOS1)-derived nitric oxide (NO) promotes oxLDL uptake and enhances the release of pro-inflammatory cytokines by macrophages [31]. In this study, we determined the effects of PAV on foam cell formation. Without oxLDL induction, PAV at concentrations of 100 - 400 µg/mL and 20 - 40 µM Svt did not induce lipid accumulation in treated cells of both NGM and HGM (**Figure 1**). The co-treatment of oxLDL and LPS resulted in lipid accumulation in RAW264.7 cells (**Figure 2**). For oxLDL, LPS and Svt co-treatment, the lipid accumulation was decreased when compared with that of oxLDL and LPS co-treatment alone in both NGM and HGM. Co-treatment of oxLDL, LPS and PAV (100 - 200 µg/mL) reduced lipid accumulation in foam cells slightly for both NGM and HGM, while oxLDL and LPS co-treatment alone showed lipid droplets accumulation in some cells (**Figure 2**). Lipid storage in foam cells with the presence or absence of 50 µg/mL oxLDL and 0.5 µg/mL LPS co-treatment in NGM and HGM was measured by Oil-red-O absorption (**Figure 3**). In the absence of 50 µg/mL oxLDL, PAV and Svt showed no statistical difference in lipid storage between NGM and HGM. However, in the presence of 50 µg/mL oxLDL and 0.5 µg/mL LPS, there was higher absorption than in the absence of 50 µg/mL oxLDL and 0.5 µg/mL LPS. Svt treatment could significantly decrease the absorption of lipid storage in both NGM and HGM. Simvastatin may enhance ox-LDL-induced macrophage autophagy and attenuate lipid aggregation [32]. However, PAV treatment showed no statistical difference in lipid storage between NGM and HGM. PAV might affect lipid aggregation or receptors for ox-LDL induced macrophage foam cell formation.

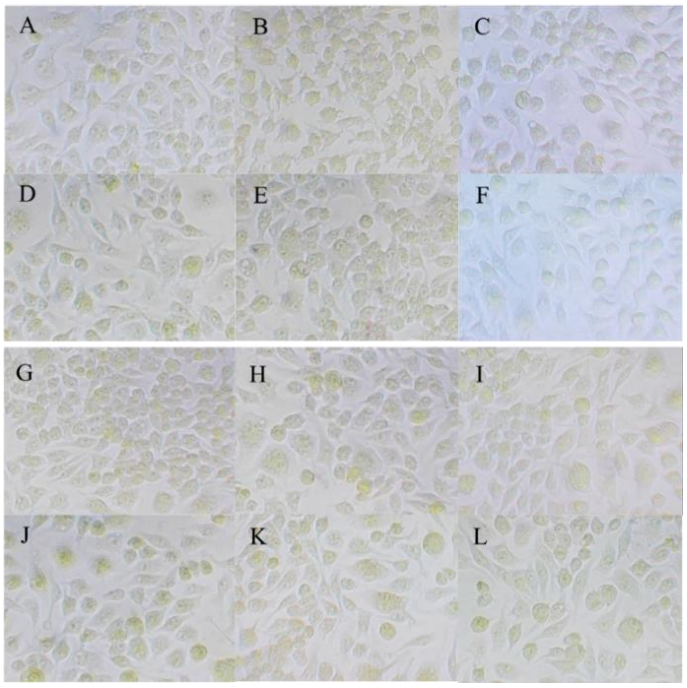

Figure 1 Oil Red O staining of RAW264.7 cells in NGM and HGM after treatment with PAV and Svt. (A) NGM, (B) 20 µM Svt in NGM, (C) 40 µM Svt in NGM, (D) 100 µg/mL PAV in NGM, (E) 200 µg/mL PAV in NGM, (F) 400 µg/mL PAV in NGM, (G) HGM, (H) 20 µM Svt in HGM, (I) 40 µM Svt in HGM, (J) 100 µg/mL PAV in HGM, (K) 200 µg/mL PAV in HGM, (L) 400 µg/mL PAV in HGM.

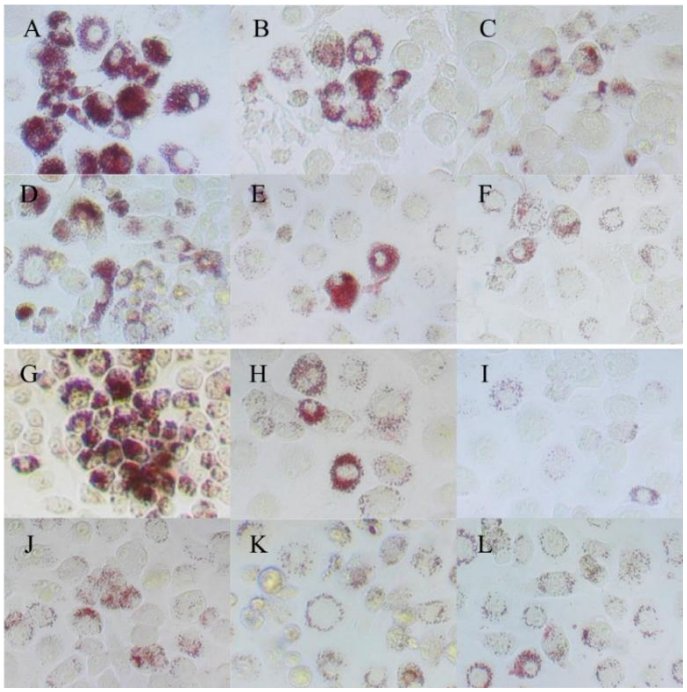

Figure 2 Oil Red O staining of RAW264.7 cells in NGM and HGM after treatment with PAV and Svt in the presence of 50 μg/mL oxLDL and 0.5 μg/mL LPS. (A) oxLDL- and LPS-contained NGM, (B) 20 μM Svt in oxLDL- and LPS-contained NGM, (C) 40 μM Svt in oxLDL- and LPS-contained NGM, (D) 100 μg/mL PAV in oxLDL- and LPS-contained NGM, (E) 200 μg/mL PAV in oxLDL- and LPS-contained NGM, (F) 400 μg/mL PAV in oxLDL- and LPS-contained NGM, (G) oxLDL- and LPS-contained HGM, (H) 20 μM Svt in oxLDL- and LPS-contained HGM, (I) 40 μM Svt in oxLDL- and LPS-contained HGM, (J) 100 μg/mL PAV in oxLDL- and LPS-contained HGM, (K) 200 μg/mL PAV in oxLDL- and LPS-contained HGM, (L) 400 μg/mL PAV in oxLDL- and LPS-contained HGM.

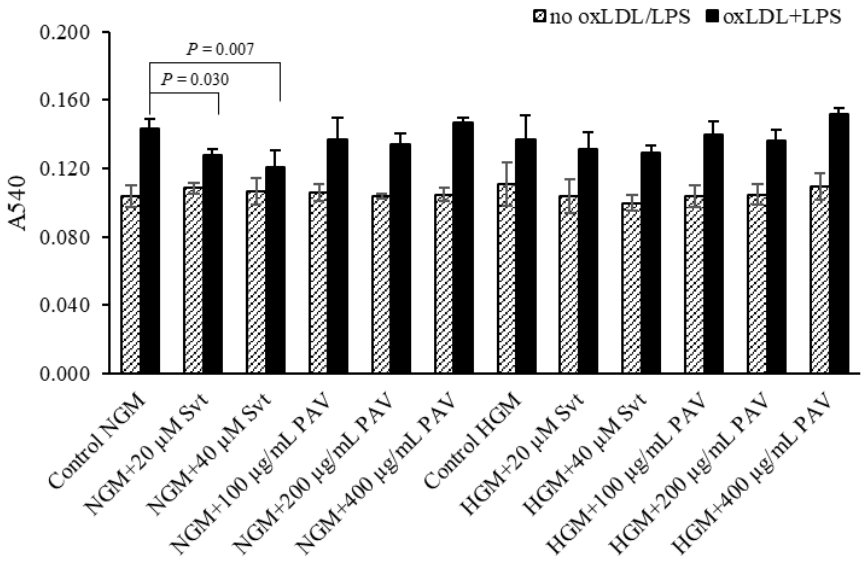

Figure 3 Oil Red O absorption from lysed foam cells after treatment with PAV and Svt in the presence or absence of 50 μg/mL oxLDL and 0.5 μg/mL LPS in NGM and HGM. Represents a significant difference in absorption for each concentration of PAV and Svt compared with control (p-value < 0.05).

Gene expression

OxLDL has also been shown to be a powerful regulator of macrophage gene expression. Several genes are involved in the inflammatory response, including TNF-α that is known to be modulated by exposure to oxLDL. Moreover, macrophages internalize oxLDL by several scavenger receptors (SRs) such as SR-A1 and LOX-1, resulting in lipid accumulation and transformation into foam cells [4]. In NGM conditions, with and without oxLDL, oxLDL+LPS induction, PAV at concentration of 100 - 400 µg/mL did not affect the expression of LOX-1 and SR-A1 compared with control, except for 10 µM Svt that significantly decreased the SR-A1 expression in oxLDL and LPS co-treatment. Interestingly, 400 µg/mL PAV significantly decreased the TNF-α expression in a dose-dependent manner compared to control with oxLDL, oxLDL+LPS induction. This study revealed that TNF-α was significantly decreased in the third condition with 10 µM Svt compared to the control group (**Figure 4**).

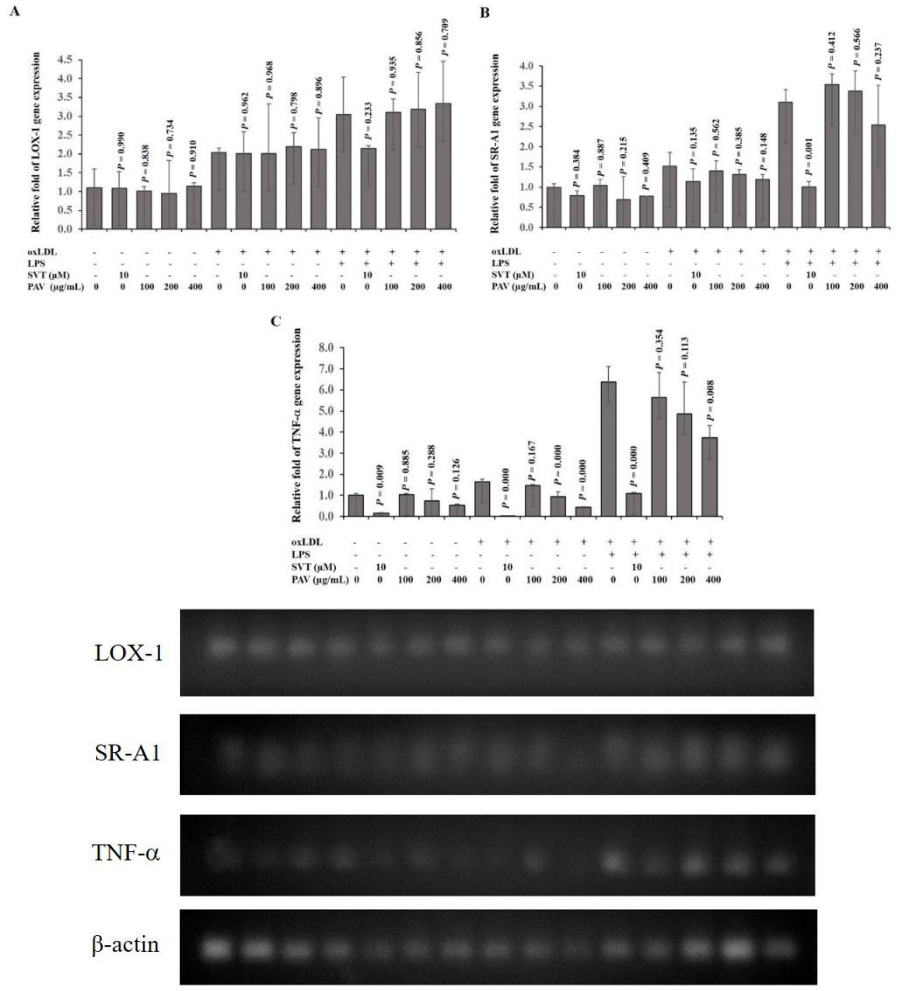

Figure 4 The effect of PAV and Svt on oxLDL and oxLDL+LPS induced LOX-1 (A), SR-A1 (B) and TNF-α (C) expression in RAW 264.7 cells in the NGM condition. $p < 0.05$ vs. control group of without oxLDL and LPS, control group of with oxLDL or control group of oxLDL and LPS. One-way ANOVA analysis was used to calculate *p*-values. The bars represent mean ± SD.

Anti-diabetic drugs including insulin up-regulate the TNF-α gene expression in mild or severe glucose load [33]. In HGM conditions, without oxLDL induction, 200 µg/mL PAV significantly decreased the LOX-1 but significantly increased TNF-α expressions, while 400 µg/mL PAV significantly increased the LOX-1 and SR-A1 expressions, and 10 µM Svt significantly increased the SR-A1 and TNF-α expressions. In oxLDL induction, 10 µM Svt significantly increased the SR-A1 expression. The 400 µg/mL PAV significantly increased

the LOX-1. The 100 - 400 μg/mL PAV significantly increased SR-A1 gene expressions in a dose-dependent manner. However, the 200 - 400 μg/mL PAV significantly decreased TNF-α gene expressions in a dose-dependent manner. In oxLDL and LPS co-treatment, 10 μM Svt significantly increased the TNF-α, but decreased the SR-A1 gene expression. The 200 - 400 μg/mL PAV significantly increased the LOX-1 expressions in a dose-dependent manner. The 100 - 400 μg/mL PAV significantly decreased the SR-A1 expression. Only 400 μg/mL PAV significantly decreased TNF-α gene expression (**Figure 5**). These results might indicate the effect of the antioxidative, NO production inhibitory and anti-inflammatory properties of the plants contained in PAV [15,34-35]. Tanaka *et al.* [35] reported that *Terminalia bellirica* extract treatment resulted in significant decreases of the mRNA expression of TNF-α, and LOX-1 in THP-1 macrophages. Allicin from garlic (*Allium sativum*) showed an anti-atherogenic effect via antioxidative activity, lipoprotein modification and inhibition of LDL uptake and degradation by macrophages [36]. Addition of *Coriandrum sativum* L. extract to oxLDL treated macrophages significantly reduced intracellular cholesterol accumulation [37]. Moreover, the possible mechanism of anti-atherosclerotic action of the piper species could be by lowering the plasma lipid concentration and scavenging the reactive oxygen species, which may oxidize the LDL-C, resulting foam cell deposition [38].

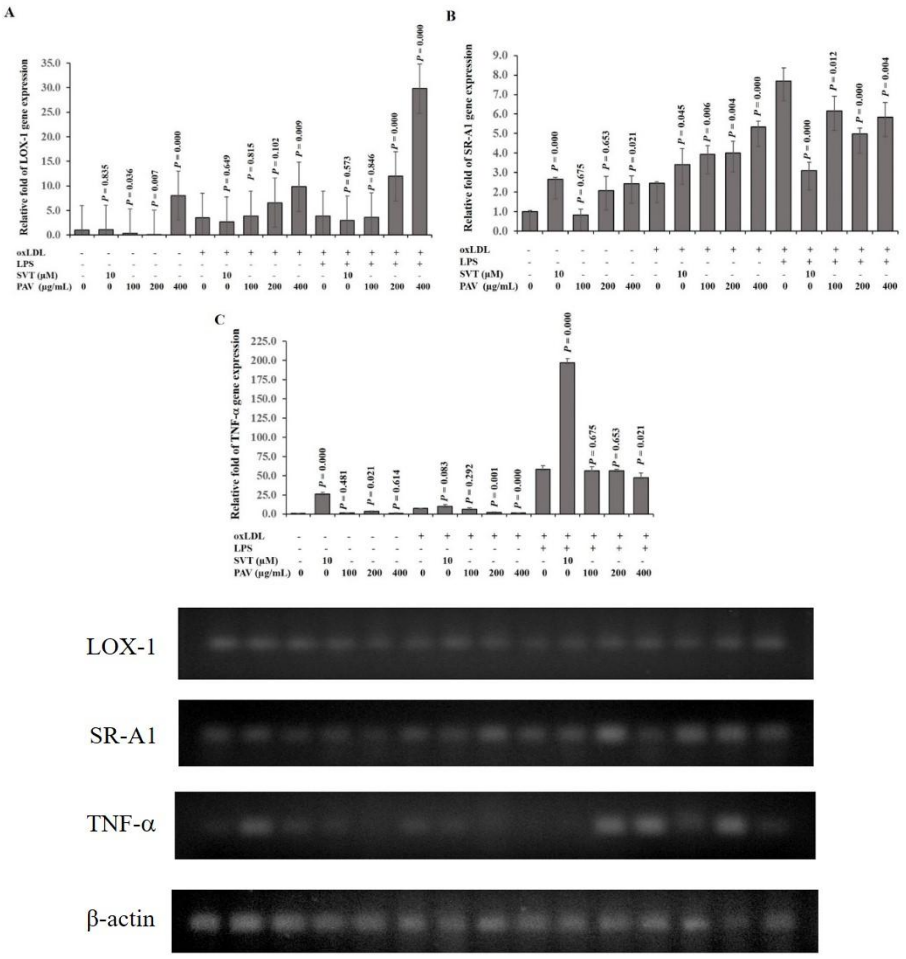

Figure 5 The effect of PAV and Svt on oxLDL and oxLDL+LPS induced LOX-1 (A), SR-A1 (B) and TNF-α (C) expression in RAW 264.7 cells in the HGM condition. $p < 0.05$ vs. control group absent oxLDL+LPS, control group of present oxLDL or control group of present oxLDL+LPS. One-way ANOVA analysis was used to calculate *p*-values. The bars represent mean ± SD.

TNF-α production

In the TNF-α producing study, with and without oxLDL or oxLDL+LPS induction, 400 μg/mL PAV significantly decreased the production of TNF-α compared with each control in both NGM and HGM conditions (**Figure 6**). These results were correlated with TNF-α gene expression. PAV could inhibit NO production in NGM and HGM [15] that might decrease the oxLDL uptake and reduce the release of TNF-α by macrophages [31]. However, the combination of pioglitazone and metformin as well as insulin up-regulated TNF-α protein secretion *in vitro* in mild diabetic status and highly up-regulated it in severe diabetic status [33]. Svt could significantly increase this cytokine production in both with and without oxLDL treatments, as well as with oxLDL+LPS treatments in the NGM condition, but Svt could significantly decrease TNF-α production in both with and without oxLDL treatments in the HGM condition. However, TNF-α production of Svt treatment did not show significant difference from the control group in oxLDL+LPS induction (**Figure 6**), even though TNF-α gene expression was increased.

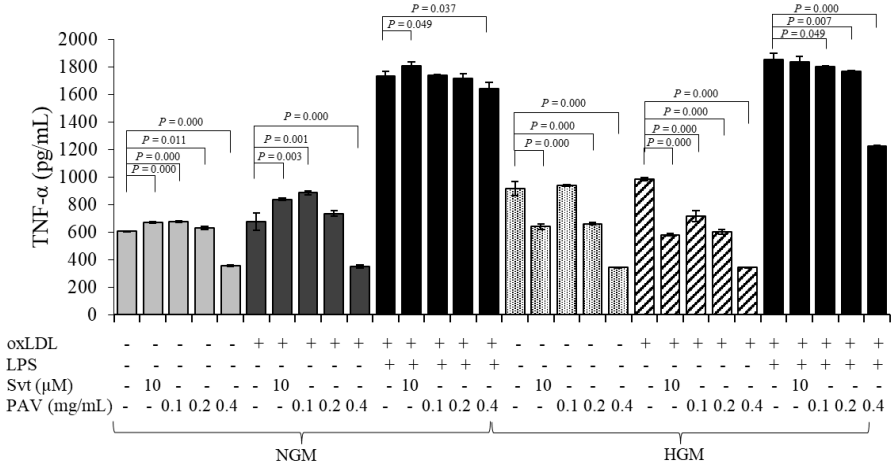

Figure 6 The effect of PAV and Svt on oxLDL and oxLDL+LPS induced TNF-α protein expression in RAW 264.7 cells in both NGM and HGM condition. $p < 0.05$ vs. control group of absent oxLDL+LPS, control group of present oxLDL or control group of present oxLDL+LPS. One-way ANOVA analysis was used to calculate *p*-values. The bars represent mean ± SD.

Ontology of identified proteins

By shotgun proteomics analysis, 7,192 differential expressed proteins in macrophages that were cultured in 6 conditions of HGM, including HGM, HGM+400 μg/mL PAV, HGM+oxLDL, HGM+oxLDL+400 μg/mL PAV, HGM+oxLDL+LPS and HGM+oxLDL+LPS+400 μg/mL, PAV were identified. Functional prediction results showed that theses high glucose response proteins are involved in many biological processes (e.g. cellular process, metabolic process, biological regulation, cellular component organization or biogenesis, response to stimulus, localization, signaling and developmental process). These identified proteins were predicted to function in cellular process (26%), metabolic process (15%), biological regulation (14%), cellular component organization or biogenesis (9%), response to stimulus (9%), localization (7%), signaling (6%), developmental process (4%), multicellular organismal process (4%), biological adhesion (2%), immune system process (1%), multi-organism process (1%), reproductive process (1%), reproduction (1%) and locomotion (1%) (**Figure 7**).

Proteins detected only in high glucose conditions in the presence or absence of PAV

To identify biochemical pathways of PAV relevant proteins associated with glucose mechanism, a total of 42 proteins were expressed only in glucose mechanism, including HGM and HGM+400 μg/mL PAV (**Figure 8**, **Table S1**). These proteins were analyzed for their interactions with glucose, insulin and

metformin treatment of diabetes and phytochemicals contained in PAV (caffeic acid and gallic acid) [15] according to the online STITCH 4.0 database. Caffeic acid is a safe and potent agent against diabetes that acts as an effective antioxidant in reducing the serum glucose, lipid profile and atherogenic indices [39]. Gallic acid suppresses hepatic lipid accumulation, apoptosis, and inflammation caused by the interaction between hepatocytes and macrophages [40]. Therefore, this reported protein marker connecting with PAV phytochemicals might be associated with the inflammation and lipid pathways **(**foam cell formation**)** when using the PAV in high glucose medium. As shown in **Figure 9**, the 5 candidate proteins including tyrosine-protein kinase receptor (Igf1r), 5-hydroxytryptamine (Serotonin) receptor 1B (Htr1b), Unconventional myosin-Ia (Brush border myosin I) (BBM-I) (BBMI) (Myosin I heavy chain) (MIHC) (Myo1a), Complement component 7 (C7) and Serine/threonine-protein kinase SIK3 (Sik3) showed an interaction network with glucose or drug treatment of diabetics or phenolics contained in PAV. Four specific proteins might play a pivotal role in the observed phenotype and be functionally relevant to the disease pathway.

For the glucose pathway, we found tyrosine-protein kinase receptor (lgf1r) in both HGM and HGM+400 μg/mL PAV conditions, which linked with glucose, insulin and metformin. Insulin controls a wide variety of biological processes by acting on two closely related tyrosine kinase receptors [41]. Tyrosine-protein kinase receptor might be the signaling mechanism of PAV for activation of the tyrosine kinase activity of the insulin receptor. This receptor represents an essential step in the insulin signal transduction across the plasma membrane of target cells, as well as metformin that potentiates the effect of insulin on glucose transport at sites beyond insulin receptor binding and phosphorylation [42]. In addition, serotonin 5-Hydroxytryptamine (5-HT) receptors play a role in diabetes mellitus and elicit its beneficial effects on glucose metabolism through serotonylation of Rab4, which likely represents the converging point between the insulin and the 5-HT signaling cascades [43]. Therefore, PAV may affect both tyrosine-protein kinase receptors and 5-HT receptors that are related to glucose metabolism.

For the lipid metabolism pathway, salt-inducible kinases (SIKs) belong to the AMP-activated protein kinase (AMPK) family, and function mainly to be involved in regulating energy response-related physiological processes, such as gluconeogenesis and lipid metabolism [44]. Members of the SIK family are emerging as the important modulators of key processes such as insulin signaling in adipocytes [45]. SIK3 also regulates cholesterol and bile acid metabolism by combining with retinoic acid metabolism and might alter energy storage in mice. Inhibition of fatty acid synthesis was observed in Sik3 KO mice [46]. In addition, 5-HT increased the lipid accumulation in human and mouse fat cells [47]. Moreover, complement component 7 (CC7) is a marker of complement activity, and associates to acute coronary syndrome (ACS) [48]. The interaction of C7 with the α-chain of C5b in C5b6 results in a C5b-7 complex, with an amphiphilic transformation of the C7 molecule to produce a complex with high affinity for lipids [49]. CC7 binds to the C5bC6 complex, which is a part of the terminal complement complex (TCC/C5b-9) [48]. The accumulation of either oxidized or enzymatically modified LDL-bound to C-reactive protein or not—prompts complement activation and leads to the assembly of the terminal complement C5b-9 complex in the atherosclerotic lesion [50]. Therefore, 400 μg/mL PAV in the HGM condition, supplemented with oxLDL or oxLDL+LPS, significantly increased the LOX-1 expression (**Figure 4**), leading to distribution of lipid accumulation in RAW264.7 macrophage cells in HGM+oxLDL+LPS+400 μg/mL PAV (**Figure 2**). These results might indicate the role of SIK3, 5-HT and CC7 protein in regulating lipid metabolism in macrophages after being treated with 400 μg/mL PAV in the HGM condition.

For inflammatory pathways, SIKs regulate cytokine production in macrophages are complex, and the specific role of each SIK isoform seems to vary among different cytokines. SIK3 showed little effect on IL-10 production while having a significant impact on the production of pro-inflammatory cytokines in response to LPS [51]. Inhibiting SIK2 and SIK3 in mature macrophages induces a population of macrophages producing high levels of IL-10 and low levels of pro-inflammatory cytokines including TNF-α [51]. SIK inhibitors compromised CRTC3

phosphorylation in TLR-stimulated macrophages, leading to an increase in CREB-dependent gene expression, including IL-10, and reduced pro-inflammatory cytokine expression, such as TNF-α [52]. Some evidence also suggests that SIK3 can inhibit toll-like receptor (TLR) signaling through IKK-mediated NF-κB signaling pathways. SIK3 may play an important role in promoting anti-inflammatory phenotypes [53]. Moreover, 400 µg/mL PAV in HGM conditions, supplemented with oxLDL or oxLDL+LPS, significantly decreased the TNF-α expression that might correlate with the SIK3 protein in HGM and HGM+PAV conditions.

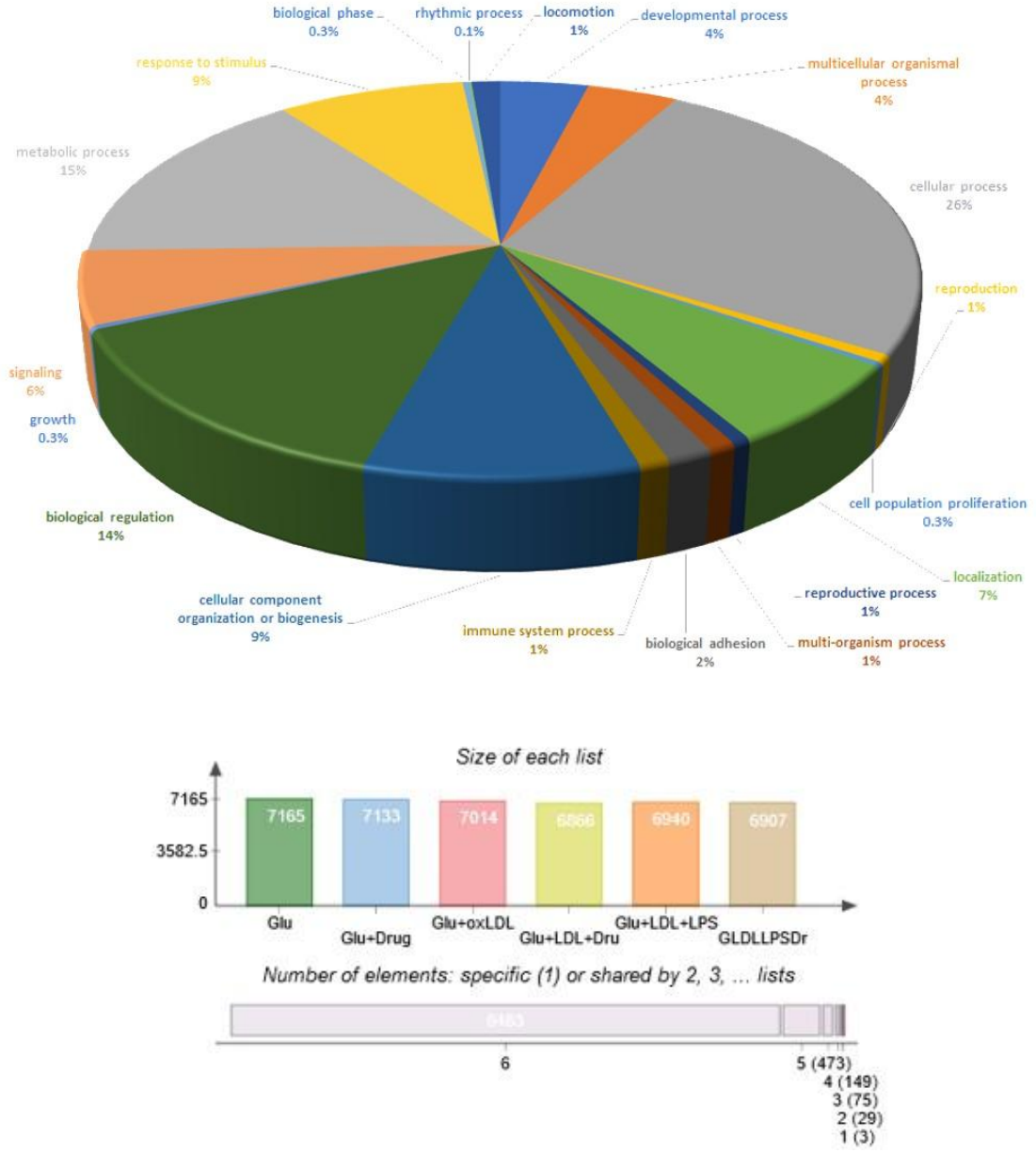

Figure 7 Distribution of gene ontology (GO) terms in the Biological process category of 7,192 differential expressed proteins in macrophages from 6 conditions of HGM including Glu (being HGM), Glu+Drug (being HGM+400 µg/mL PAV), Glu+oxLDL (being HGM+oxLDL), Glu+LDL+Dru (being HGM+oxLDL+400 µg/mL PAV), Glu+LDL+LPS (being HGM+oxLDL+LPS) and GluLDLLPSDr (being HGM+oxLDL+LPS+400 µg/mL PAV).

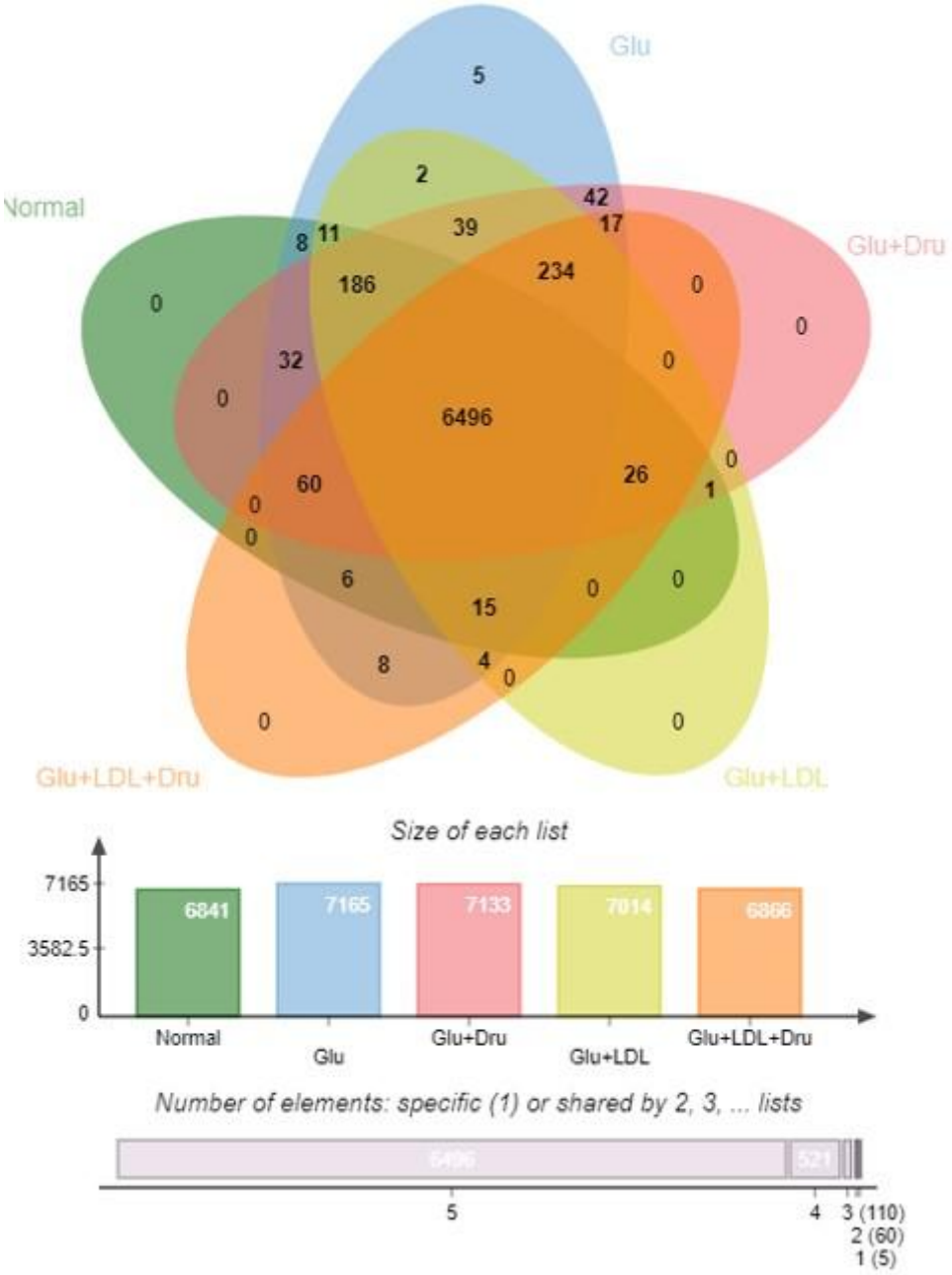

Figure 8 Venn diagram showing the number of expressed proteins detected in RAW264.7 macrophages for 5 conditions analyzed by shotgun proteomics. Normal (being control of no glucose), Glu (being HGM), Glu+Dru (being HGM+400 µg/mL PAV), Glu+LDL (being HGM+oxLDL) and Glu+LDL+Dru (being HGM+oxLDL+400 µg/mL PAV) were the effect of PAV on HGM or HGM+oxLDL conditions.

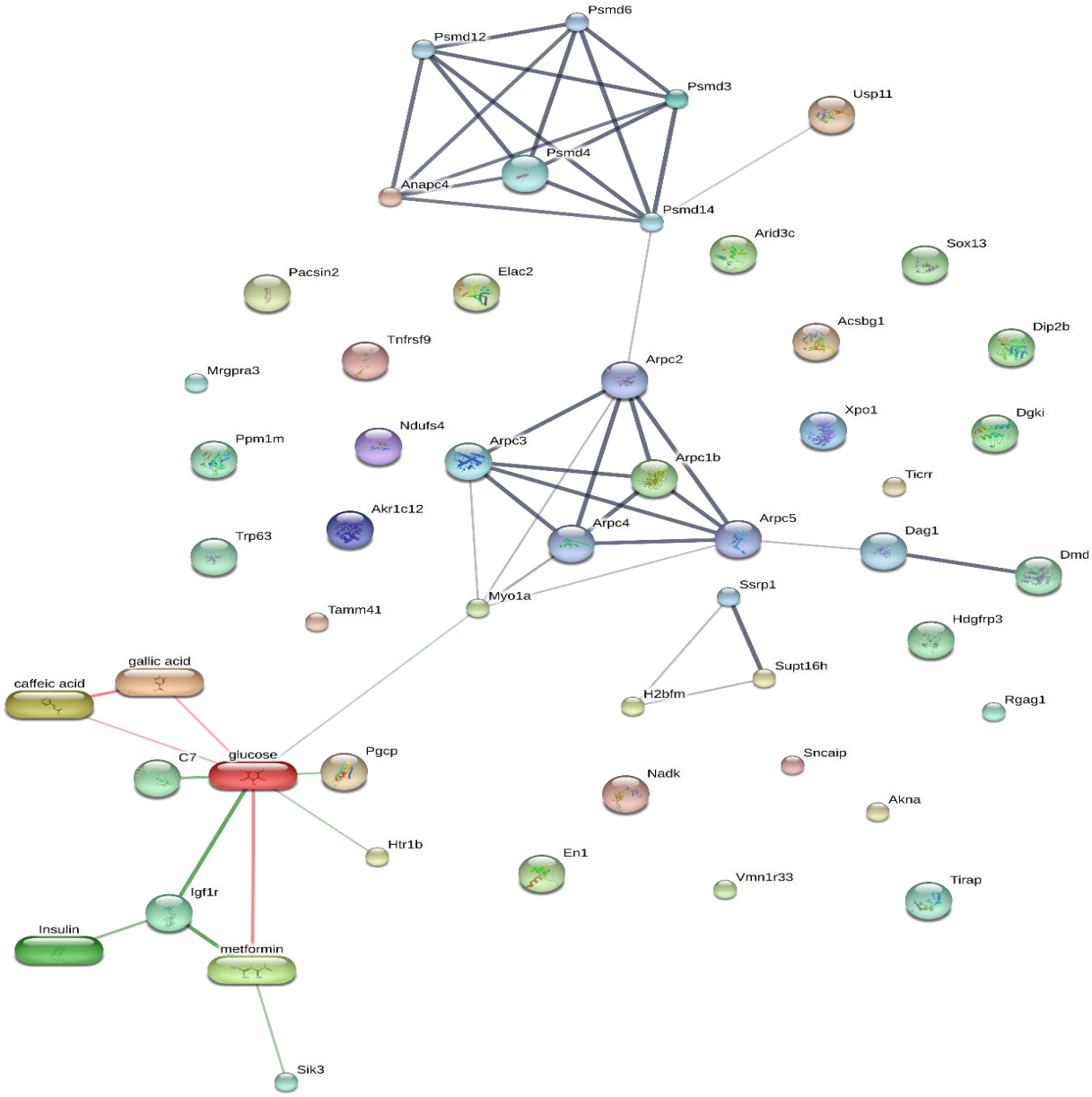

Figure 9 Predicted interactions between glucose, diabetic drug, phenolics contained in PAV and RAW264.7 macrophage proteins that were detected only in HGM and HGM+400 µg/mL PAV. Modes of action are shown by different color lines.

Conclusions

In conclusion, results in this study indicate that PAV slightly suppressed lipid accumulation in foam cells, but when increasing the PAV concentration (200 - 400 µg/mL) the lipid accumulation in cells was slightly increased and spread in cells all over the culture wells. These results correlated with gene expression results. PAV could up-regulate gene expressions of oxLDL receptors including LOX-1. However, PAV down-regulated pro-inflammatory cytokine genes, including TNF-α and decreased the cytokine production in the oxLDL+LPS condition in both NGM and HGM. For oxLDL-induced foam cell formation, PAV slightly suppressed lipid accumulation in foam cells. But when increasing PAV concentration (200 - 400 µg/mL) the lipid accumulation in cells was slightly increased and spread in the cells all over the culture wells. These results correlate with gene expression results. PAV could up-regulate gene expression of oxLDL receptors including LOX-1. However, PAV down-regulated pro-

inflammatory cytokine genes including TNF-α and decreased the cytokine production in the oxLDL+LPS condition in both NGM and HGM. Forty-two proteins were uniquely detected in HGM and HGM+400 µg/mL PAV conditions. In interactions among glucose, insulin and metformin treatment diabetes, phytochemicals in PAV and 4 specific proteins were demonstrated. PAV might potentiate the insulin on glucose transport that relates to tyrosine kinase receptors. Moreover, PAV might affect the 5-Hydroxytryptamine receptors on macrophages, and play important roles in insulin secretion, glucose metabolism and lipid accumulation. The CC7 that is a part of the terminal complement complex C5b-9 in the atherosclerotic lesion was found. SIK3 protein might reduce pro-inflammatory cytokine expression in the RAW264.7 macrophage or regulate lipid metabolism in macrophages. Therefore, PAV treatment under high glucose conditions correlates with the reduction of pro-inflammatory cytokines, and is associated with lipid accumulation on foam cells formation in RAW264.7 macrophages.

Acknowledgements

This work was financially supported by The Thai Traditional Medical Knowledge Fund, Department of Thai Traditional and Alternative Medicine (Grant no. 27/2563). Thank you to the Faculty of Agricultural Technology, Burapha University Sakaeo Campus, Thailand for instrumental facilities.

CRediT author statement

Bung-on Prajanban: Methodology; Investigation; Writing - Original draft preparation; Writing - Review and Editing. **Orapun Jaisamut**: Methodology; Investigation. **Sittiruk Roytrakul**: Methodology; Investigation. **Niramai Fangkrathok**: Conceptualization; Methodology; Investigation; Writing – Original draft preparation; Writing – Review and Editing.

References

[1] A Poznyak, AV Grechko, P Poggio, VA Myasoedova, V Alfieri and AN Orekhov. The diabetes mellitus-atherosclerosis connection: the role of lipid and glucose metabolism and chronic inflammation. *International Journal of Molecular Sciences* 2020; **21(5)**, 1835.

[2] ZC Wang, JO Machuki, MZ Li, KX Li and HJ Sun. A narrative review of plant and herbal medicines for delaying diabetic atherosclerosis: an update and future perspectives. *Reviews in Cardiovascular Medicine* 2021; **22(4)**, 1361-1381.

[3] C Alan and KE Bornfeldt. Diabetes and atherosclerosis: is there a role for hyperglycemia? *Journal of Lipid Research* 2009; **50(S)**, S335-S339.

[4] A Pirillo, GD Norata and AL Catapano. LOX-1, OxLDL, and atherosclerosis. *Mediators of Inflammation* 2013; **2013**, 152786.

[5] DF Schaeffer, M Riazy, KS Parhar, JH Chen, V Duronio, T Sawamura and UP Steinbrecher. LOX-1 augments oxLDL uptake by lysoPC-stimulated murine macrophages but is not required for oxLDL clearance from plasma. *Journal of Lipid Research* 2009; **50(8)**, 1676-1684.

[6] L Li, T Sawamura and G Renier. Glucose enhances human macrophage LOX-1 expression: role for LOX-1 in glucose-induced macrophage foam cell formation. *Circulation Research* 2004; **94(7)**, 892-901.

[7] M Nagase, J Abe, K Takahashi, J Ando, S Hirose and T Fujita. Genomic organization and regulation of expression of the lectin-like oxidized low-density lipoprotein receptor (LOX-1) gene. *The Journal of Biological Chemistry* 1998; **273(50)**, 33702-33707.

[8] N Kume, T Murase, H Moriwaki, T Aoyama, T Sawamura, T Masaki and T Kita. Inducible expression of lectin-like oxidized LDL receptor-1 in vascular endothelial cells. *Circulation Research* 1998; **83(3)**, 322-327.

[9] M Hashizume and M Mihara. Blockade of IL-6 and TNF-α inhibited oxLDL-induced production of MCP-1 via scavenger receptor induction. *European Journal of Pharmacology* 2012; **689(1-3)**, 249-254.

[10] J Persson, J Nilsson and MW Lindholm. Interleukin-1beta and tumor necrosis factor-alpha impede neutral lipid turnover in macrophage-derived foam cells. *BMC Immunology* 2008; **9(1)**, 1-11.

[11] M Hashizume and M Mihara. Atherogenic effects of TNF-α and IL-6 via up-regulation of scavenger receptors. *Cytokine* 2012; **58(3)**, 424-430.

[12] CH Kim, KA Han, HJ Oh, KE Tan, R Sothiratnam and A Tjokroprawiro. Safety, tolerability, and efficacy of metformin extended-release oral antidiabetic therapy in patients with type 2 diabetes: an observational trial in Asia. *Journal of Diabetes* 2012; **4(4)**, 395-406.

[13] C Andrade, NGM Gomes, S Duangsrisai, PB Andrade, DM Pereira and P Valentão. Medicinal plants utilized in Thai traditional medicine for diabetes treatment: Ethnobotanical surveys, scientific evidence and phytochemicals. *Journal of Ethnopharmacology* 2020; **263**, 113177.

[14] P Peungvicha, O Vallisuta, S Mangmool, T Sirithamwanich and R Sirithamwanich. Anti-hyperglycemic effect and subchronic toxicity of the combined extract from Sattagavata-Mathurameha-Tubpikarn anti-diabetic herbal formulae. *Thai Journal of Pharmaceutical Sciences* 2018; **42(1)**, 6-13.

[15] B Prajanban, O Jaisamut and N Fangkrathok. Quality control, cytotoxicity and inhibitory effect on nitric oxide production of Pathavi Apo Vayo formulary extract. *Huachiew Chalermprakiet Science and Technology Journal* 2022; **8(2)**, 92-106.

[16] R Li, T Chaicherdsakul, V Kunathigan, S Roytrakul, A Paemanee and S Kittisenachai. Shotgun proteomic analysis of germinated rice (*Oryza sativa* L.) under salt stress. *Applied Science and Engineering Progress* 2020; **13(1)**, 76-85.

[17] H Kim, J Chen, B Prescott, ME Walker, ME Grams, B Yu, RS Vasan, JS Floyd, N Sotoodehnia, NL Smith, DE Arking, J Coresh and CM Rebholz. Plasma proteins associated with plant-based diets: results from the atherosclerosis risk in communities (ARIC) study and framingham heart study (FHS). *Clinical Nutrition* 2024; **43(8)**, 1929-1940.

[18] MR Rooney, J Chen, JB Echouffo-Tcheugui, KA Walker, P Schlosser, A Surapaneni, O Tang, J Chen, CM Ballantyne, E Boerwinkle, CE Ndumele, RT Demmer, JS Pankow, PL Lutsey, LE Wagenknecht, Y Liang, X Sim, R Dam, ES Tai, ME Grams, …, J Coresh. Proteomic predictors of incident diabetes: Results from the atherosclerosis risk in communities (ARIC) study. *Diabetes Care* 2023; **46(4)**, 733-741.

[19] B Huang, M Jin, H Yan, Y Cheng, D Huang, S Ying and L Zhang. Simvastatin enhances oxidized-low density lipoprotein-induced macrophage autophagy and attenuates lipid aggregation. *Molecular Medicine Reports* 2015; **11(2)**, 1093-1098.

[20] X Yang, M Yin, L Yu, M Lu, H Wang, F Tang and Y Zhang. Simvastatin inhibited oxLDL-induced proatherogenic effects through calpain-1-PPARγ-CD36 pathway. *Canadian Journal of Physiology and Pharmacology* 2016; **94(12)**, 1336-1343.

[21] ZH Wu, YQ Chen and SP Zhao. Simvastatin inhibits ox-LDL-induced inflammatory adipokines secretion via amelioration of ER stress in 3T3-L1 adipocyte. *Biochemical and Biophysical Research Communications* 2013; **432(2)**, 365-369.

[22] T Hu, B Chen, S Zhou and J Mao. Simvastatin inhibits inflammatory response in lipopolysaccharide (LPS)-stimulated RAW264.7 macrophages through the microRNA-22/Cyr61 axis. *International Journal of Clinical and Experimental Pathology* 2018; **11(8)**, 3925-3933.

[23] M Rahmati-Yamchi, S Ghareghomi, G Haddadchi, M Milani, M Aghazadeh and H Daroushnejad. Fenugreek extract diosgenin and pure diosgenin inhibit the hTERT gene expression in A549 lung cancer cell line. *Molecular Biology Reports* 2014; **41(9)**, 6247-6252.

[24] G Tian, D Wilcockson, VH Perry, PM Rudd, RA Dwek, FM Platt and N Platt. Inhibition of alpha-glucosidases I and II increases the cell surface expression of functional class A macrophage scavenger receptor (SR-A) by extending its half-life. *The Journal of Biological Chemistry* 2004; **279(38)**, 39303-39309.

[25] N Fangkrathok, J Junlatat and B Sripanidkulchai. *In vivo* and *in vitro* anti-inflammatory activity of *Lentinus polychrous* extract. *Journal of Ethnopharmacology* 2013; **147(3)**, 631-637.

[26] S Tyanova, T Temu, P Sinitcyn, A Carlson, MY Hein, T Geiger, M Mann and J Cox. The Perseus computational platform for comprehensive

analysis of proteomics data. *Nature Methods* 2016; **13(9)**, 731-740.

[27] EA Howe, R Sinha, D Schlauch and J Quackenbush. RNA-Seq analysis in MeV. *Bioinformatics* 2011; **27(22)**, 3209-3210.

[28] H Mi, A Muruganujan, D Ebert, X Huang and PD Thomas. PANTHER version 14: More genomes, a new PANTHER GO-slim and improvements in enrichment analysis tools. *Nucleic Acids Research* 2019; **47(D1)**, D419-D426.

[29] P Bardou, J Mariette, F Escudié, C Djemiel and C Klopp. jvenn: An interactive Venn diagram viewer. *BMC Bioinformatics* 2014; **15(1)**, 293.

[30] D Szklarczyk, A Santos, C von Mering, LJ Jensen, P Bork and M Kuhn. STITCH 5: augmenting protein-chemical interaction networks with tissue and affinity data. *Nucleic Acids Research* 2016; **44(D1)**, D380-D384.

[31] A Roy, U Saqib, K Wary and MS Baig. Macrophage neuronal nitric oxide synthase (NOS1) controls the inflammatory response and foam cell formation in atherosclerosis. *International Immunopharmacology* 2020; **83(1)**, 106382.

[32] B Huang, M Jin, H Yan, Y Cheng, D Huang and S Ying. Simvastatin enhances oxidized-low density lipoprotein-induced macrophage autophagy and attenuates lipid aggregation. *Molecular Medicine Reports* 2015; **11(2)**,1093-1098.

[33] M Saxena, D Ali, DR Modi, MHA Almarzoug, SA Hussain and S Manohrdas. Association of *TNF-α* gene expression and release in response to anti-diabetic drugs from human adipocytes *in vitro*. *Diabetes, Metabolic Syndrome and Obesity: Targets and Therapy* 2020; **13**, 2633-2640.

[34] A Ihantola-Vormisto, J Summanen, H Kankaanranta, H Vuorela, ZM Asmawi and E Moilanen. Anti-inflammatory activity of extracts from leaves of *Phyllanthus emblica*. *Planta Medica* 1997; **63(6)**, 518-524.

[35] M Tanaka, Y Kishimoto, E Saita, N Suzuki-Sugihara, T Kamiya, C Taguchi, K Iida and K Kondo. *Terminalia bellirica* extract inhibits low-density lipoprotein oxidation and macrophage inflammatory response *in vitro*. *Antioxidants* 2016; **5(2)**, 20.

[36] A Gonen, D Harats, A Rabinkov, T Miron, D Mirelman, M Wilchek, L Weiner, E Ulman, H Levkovitz, D Ben-Shushan and A Shaish. The antiatherogenic effect of allicin: possible mode of action *Pathobiology* 2005; **72(6)**, 325-334.

[37] D Patel, S Desai, T Gajaria, R Devkar and AV Ramachandran. *Coriandrum sativum* L. seed extract mitigates lipotoxicity in RAW 264.7 cells and prevents atherogenic changes in rats. *EXCLI Journal* 2013; **12**, 313-334.

[38] GA Agbor, JA Vinson, J Sortino and R Johnson. Antioxidant and anti-atherogenic activities of three Piper species on atherogenic diet fed hamsters. *Experimental and Toxicologic Pathology* 2012; **64(4)**, 387-391.

[39] N Oršolić, D Sirovina, D Odeh, G Gajski, V Balta, L Šver and MJ Jembrek, Efficacy of caffeic acid on diabetes and its complications in the mouse. *Molecules* 2021; **26(11)**, 3262.

[40] M Tanaka, A Sato, Y Kishimoto, H Mabashi-Asazuma, K Kondo and K Iida. Gallic acid inhibits lipid accumulation via AMPK pathway and suppresses apoptosis and macrophage-mediated inflammation in hepatocytes. *Nutrients* 2020; **12(5)**, 1479.

[41] J Boucher, A Kleinridders and CR Kahn. Insulin receptor signaling in normal and insulin-resistant states. *Cold Spring Harbor Perspectives in Biology* 2014; **6(1)**, a009191.

[42] DB Jacobs, GR Hayes, JA Truglia and DH Lockwood. Effects of metformin on insulin receptor tyrosine kinase activity in rat adipocytes. *Diabetologia* 1986; **29(11)**, 798-801.

[43] R Al-Zoairy, MT Pedrini, MI Khan, J Engl, A Tschoner, C Ebenbichler, G Gstraunthaler, K Salzmann, R Bakry and A Niederwanger. Serotonin improves glucose metabolism by serotonylation of the small GTPase Rab4 in L6 skeletal muscle cells. *Diabetology and Metabolic Syndrome* 2017; **9(1)**, 1.

[44] Z Sun, Q Jiang, J Li and J Guo. The potent roles of salt-inducible kinases (SIKs) in metabolic homeostasis and tumorigenesis. *Signal Transduction and Targeted Therapy* 2020; **5(1)**, 150.

[45] M Okamoto, H Takemori and Y Katoh. Salt-inducible kinase in steroidogenesis and

adipogenesis. *Trends in Endocrinology and Metabolism* 2004; **15(1)**, 21-26.

[46] T Uebi, Y Itoh, O Hatano, A Kumagai, M Sanosaka, T Sasaki, S Sasagawa, J Doi, K Tatsumi, K Mitamura, E Morii, K Aozasa, T Kawamura, M Okumura, J Nakae, H Takikawa, T Fukusato, M Koura, M Nish, A Hamsten, …, H Takemori. Involvement of SIK3 in glucose and lipid homeostasis in mice. *PLoS One* 2012; **7(5)**, e37803.

[47] S Grès, S Canteiro, J Mercader and C Carpéné. Oxidation of high doses of serotonin favors lipid accumulation in mouse and human fat cells. *Molecular Nutrition and Food Research* 2013; **57(6)**, 1089-1099.

[48] R Aarsetøy, T Ueland, P Aukrust, AE Michelsen, RL Fuente, H Grundt, H Staines, O Nygaard and D WT Nilsen. Complement component 7 is associated with total- and cardiac death in chest-pain patients with suspected acute coronary syndrome. *BMC Cardiovascular Disorders* 2021; **21(1)**, 496.

[49] SI Vlaicu, A Tatomir, D Boodhoo, S Vesa, PA Mircea and H Rus. The role of complement system in adipose tissue-related inflammation. *Immunologic Research* 2016; **64(3),** 653-664.

[50] SI Vlaicu, A Tatomir, V Rus, AP Mekala, PA Mircea, F Niculescu and H Rus. The role of complement activation in atherogenesis: The first 40 years. *Immunologic Research* 2016; **64(1)**, 1-13.

[51] NJ Darling, R Toth, JS Arthur and K Clark. Inhibition of SIK2 and SIK3 during differentiation enhances the anti-inflammatory phenotype of macrophages. *The Biochemical journal* 2017; **474(4)**, 521-537.

[52] K Clark, KF MacKenzie, K Petkevicius, Y Kristariyanto, J Zhang, HG Choi, M. Peggie, L Plater, PGA Pedrioli, E McIver, NS Gray, JSC Arthur and P Cohen. Phosphorylation of CRTC3 by the salt-inducible kinases controls the interconversion of classically activated and regulatory macrophages. *Proceedings of the National Academy of Sciences of the United States of America* 2012; **109(42)**, 16986-16991.

[53] SY Kim, S Jeong, KH Chah, E Jung, KH Baek, ST Kim, JH Shim, E Chun and KY Lee. Salt-inducible kinases 1 and 3 negatively regulate Toll-like receptor 4-mediated signal. *Molecular Endocrinology* 2013; **27(11)**, 1958–1968.

Supplementary Materials

Table S1 Identified proteins observed only in HGM and HGM+400 μg/mL PAV.

Protein name	NCBI accession number	Gene name	Function
Tyrosine-protein kinase receptor (EC 2.7.10.1)	E9QNX9	Igf1r	signal transduction
PCI domain-containing protein	Q3U5M8	Psmd3	metabolic process
Xpo1 protein	Q921J0	Xpo1	signal transduction
Aldo-keto reductase AKR1C12	Q9R0M7	Akr1c12	metabolic process
NADH dehydrogenase [ubiquinone] iron-sulfur protein 4, mitochondrial (Complex I-18 kDa) (NADH-ubiquinone oxidoreductase 18 kDa subunit)	E9QPX3	Ndufs4	cellular process
Synphilin-1	J3QP58	Sncaip	biological regulation
CD137 antigen	Q3U3R1	Tnfrsf9	signal transduction
Uncharacterized protein	Q3TNZ1	Nadk	metabolic process
Anaphase-promoting complex subunit 4 (Cyclosome subunit 4)	Q3TI31	Anapc4	cellular process
Phosphatidate cytidylyltransferase, mitochondrial (EC 2.7.7.41) (CDP-diacylglycerol synthase) (CDP-DAG synthase) (Mitochondrial translocator assembly and maintenance protein 41 homolog) (TAM41)	Q3TUH1	Tamm41	cellular process
USP domain-containing protein	Q3T9X4	Usp11	biological regulation
Long-chain-fatty-acid-CoA ligase ACSBG1 (Fragment)	D3YZ56	Acsbg1	metabolic process
Aminopeptidase (Fragment)	Q9R1I4	Cpq Pgcp	cellular process
Treslin_N domain-containing protein	Q8C6J3	Ticrr 5730590G19Rik	cellular process
Microtubule organization protein AKNA (AT-hook-containing transcription factor)	Q80VW7	Akna Kiaa1968	biological regulation
SPT16, facilitates chromatin-remodeling subunit	G3X956	Supt16 Supt16h	cellular component
5-hydroxytryptamine (Serotonin) receptor 1B	Q0VES5	Htr1b	signal transduction
H2B histone family, member M	Q9DAB5	H2bfm 1700014N06Rik	cellular component
SH3 domain-containing protein (Fragment)	Q8BNK9	Pacsin2	cellular process
Uncharacterized protein	Q3U0M8	Elac2	cellular process
Unconventional myosin-Ia (Brush border myosin I) (BBM-I) (BBMI) (Myosin I heavy chain) (MIHC)	O88329	Myo1a Bbmi Myhl	cellular component
Homeobox protein engrailed-1 (Homeobox protein en-1) (Mo-En-1)	P09065	En1 En-1	cellular component

Protein name	NCBI accession number	Gene name	Function
AT-rich interactive domain-containing protein 3C (Arid3c protein)	B7ZP08	Arid3c	cellular component
Actin-related protein 2/3 complex subunit 1B (Fragment)	F6THG2	Arpc1b	cellular component
Transcription factor SOX-13	D3Z7I3	Sox13	cellular process
DIP2 disco-interacting protein 2 homolog B (Drosophila) (Disco-interacting protein 2 homolog B)	B2RQC7	Dip2b	cellular process
Diacylglycerol kinase (DAG kinase) (EC 2.7.1.107)	D3YWQ0	Dgki	metabolic process
Uncharacterized protein (Fragment)	Q8C9E2	Hdgfl3 Hdgfrp3	
Complement component 7	D3YXF5	C7	immune system
Dystrophin	P11531	Dmd	cellular component
Tumor protein 63 (p63)	Q3UVI3	Trp63	cellular process
Protein phosphatase 2C eta-2	B7XGC0	Ppm1m ppm1m	cellular process
Serine/threonine-protein kinase SIK3 (Fragment)	F6U6U5	Sik3	cellular process
Retrotransposon Gag-like protein 9 (Retrotransposon gag domain-containing protein 1) (Sushi-XF2)	Q32KG4	Rtl9 Gm385 Kiaa1318 Rgag1	cellular process
Toll/interleukin-1 receptor domain-containing adapter protein (TIR domain-containing adapter protein)	H3BKL1	Tirap	signal transduction
Mas-related G-protein-coupled receptor member A3	H3BKL3	Mrgpra3	signal transduction
Zinc finger MYM-type protein 4 (Fragment)	F6VYE2*	Zmym4	cellular component
Uncharacterized protein	A0A5F8MPE6	Fam90a1b	cellular process
Phosphatidate cytidylyltransferase, mitochondrial (EC 2.7.7.41) (CDP-diacylglycerol synthase) (Mitochondrial translocator assembly and maintenance protein 41 homolog)	G5E881	Tamm41 1500001M20Rik	cellular component organization
60 kDa lysophospholipase (Fragment)	A0A1Y7VIV3	Aspg	cellular process
Protein NLRC3 (Fragment)	A0A2R8VHN0	Nlrc3	immune system